NASA-TM-84583 19850007387

NASA Technical Memorandum 84583

AN EXPLORATORY STUDY OF FINITE DIFFERENCE GRIDS FOR TRANSONIC UNSTEADY AERODYNAMICS

David A. Seidel, Robert M. Bennett and Woodrow Whitlow, Jr.

December 1982

National Aeronautics and Space Administration

Langley Research Center
Hampton, Virginia 23665

AN EXPLORATORY STUDY OF FINITE DIFFERENCE GRIDS FOR TRANSONIC UNSTEADY AERODYNAMICS

David A. Seidel, Robert M. Bennett, and Woodrow Whitlow, Jr.

ABSTRACT

Unsteady aerodynamic forces are calculated by the XTRAN2L finite difference program which solves the complete two-dimensional unsteady transonic small perturbation equation. The unsteady forces are obtained using a pulse-transfer function technique which assumes the flow field behaves in a locally-linear fashion about a mean condition. Forces are calculated for a linear flat plate using the default grids from the LTRAN2-NLR, LTRAN2-HI, and XTRAN3S programs. The forces are compared to the exact theoretical values for flat plate, and grid-generated boundary and internal numerical reflections are observed to cause significant errors in the unsteady airloads. Grids are presented that alleviate the reflections while reducing computational time up to fifty-three percent and program size up to twenty-eight percent. Forces are presented for a six percent thick parabolic arc airfoil which demonstrate that the transform technique may be successfully applied to non-linear transonic flows.

NOMENCLATURE

c	airfoil chord
c_{ℓ_α}	unsteady lift force coefficient, per radian of pitch angle
c_{m_α}	unsteady pitching moment coefficient, per radian of pitch angle
C_p	pressure coefficient, $\frac{p-p_\infty}{q_\infty}$
f	airfoil contour
k	reduced frequency, $\frac{c\omega}{2V_\infty}$
M_∞	freestream Mach number
p	local static pressure
p_∞	freestream static pressure
q_∞	freestream dynamic pressure
t	time, seconds
V_∞	freestream velocity
X,Z	orthogonal coordinates in physical space
x,z	non-dimensional orthogonal coordinates in physical space $(\frac{X}{c}, \frac{Z}{c})$
α	angle of attack radians
γ	ratio of specific heats
γ^*	$2 - (2-\gamma)M_\infty^2$
δ	airfoil thickness ratio
ξ,η	orthogonal coordinates in computational space
τ	scaled time, $\frac{tV_\infty}{c}$

$\Delta\tau$	scaled time step
ϕ	perturbation velocity potential
ω	frequency of oscillation, radian/second

Subscript

o	initial or steady-state value
[ ]	denotes jump in quantity across a discontinuity

INTRODUCTION

Considerable effort is underway to develop finite difference computer codes for calculating transonic unsteady aerodynamics for flutter and other aeroelastic analyses. Difference equations are solved for a finite number of discrete points in the flow field using the techniques that have enjoyed considerable success in steady transonic flow analyses. The distribution of grid points for steady flows is a topic of active research.[1] Current practice is to map the physical domain to a finite computational region using smoothly varying stretching functions. In the calculation of unsteady flows an added concern is the dynamic behavior of the computed solution since spurious reflections due to rapid changes in grid spacing and from the outer edges of the computational domain are possible. In steady flows these effects are suppressed by iterating solutions until all dynamic phenomenon have subsided. Thus special emphasis must be given to the development and evaluation of finite difference grids for unsteady problems.

Several investigations have calculated unsteady transonic flows with finite difference techniques.[2-24] Some have used the higher level flow equations such as the Navier-Stokes equations[2], the Euler equations[3-5] and the full potential equation.[6-11] In these codes the grid is generally curvilinear, moving with the airfoil motion and quite complex in nature. In these works some variations of the internal parameters are made to verify the results but little documentation of the influence of the grid variations is given. Considerable work has been done using the low frequency versions of the transonic small perturbation (TSP) equation[12-15] including extensive flutter calculations.[16-17] Recent efforts have been directed at solving the complete TSP equation[18-24] which is applicable to higher reduced frequencies. The grid system for the TSP equations is considerably simplified as the boundary conditions are applied on a mean line representing the airfoil and wake, and the grid remains stationary. Normally a rectilinear grid is used with various spacing schemes to enhance the treatment of local phenomena.

There are some documented efforts that have shown significant effects of the grid on unsteady flow problems.[11,20,21] In ref. 11, it was demonstrated that if the grid was stretched too rapidly, such that the flow field was inadequately resolved, spurious effects can occur in the time domain solution. The investigation of ref. 20 indicated that such effects could be alleviated for the TSP equation with a more gentle stretching of the grid. During the development of the frequency domain perturbation method of refs. 21-22, significant difficulty was encountered until it was noted that an inadequate number of field points were being used to describe the wavelengths involved. Increasing the point density corrected the problem.

In the initial application of the three-dimensional TSP program XTRAN3S[23] at NASA Langley Research Center, indications of grid generated anomalies were observed. To permit economical assessment of the grid questions, a corresponding two-dimensional program, XTRAN2L, was used. The program XTRAN2L is a version of the HYTRAN2 code[16] modified to solve the complete TSP equation. The purpose of this paper is to describe both the results and the methodology used in assessing the computational grids. The approach taken is basically one of performing numerical experiments. The linearized TSP equation applied to a flat plate airfoil is used for the test case in order to permit comparisons with exact results. The airfoil is given a small prescribed pulse in angle of attack and the aerodynamic transients are calculated. A transfer function analysis using fast Fourier transforms is then used to obtain a detailed description of the aerodynamic forces in the frequency domain. This paper presents the results for various computational grids and also illustrates their use for a parabolic arc airfoil in transonic flow.

ANALYSIS TECHNIQUE AND APPLICATION

Unsteady Transonic Small Perturbation Equation

All calculations were obtained using the code XTRAN2L which solves the complete unsteady transonic small perturbation (TSP) potential equation

$$\frac{k^2 M_\infty^2}{\delta^{2/3}} \phi_{\tau\tau} + \frac{2kM_\infty^2}{\delta^{2/3}} \phi_{\xi\tau} = \left\{ \frac{1-M_\infty^2}{\delta^{2/3}} - M_\infty^2 (\gamma^*+1)\phi_\xi \right\} \phi_{\xi\xi} + \phi_{\eta\eta} \qquad (1)$$

where $\gamma^* = 2 - (2-\gamma)M_\infty^2$, which is based on the scaling used in the LTRAN2-NLR program.[14] The airfoil flow tangency and trailing edge conditions are applied on the $\eta = 0$ line and, in the small perturbation approximation, become

$$\phi_\eta = f_\xi + kf_\tau \quad ; \eta = \mp 0,\ 0 \le \xi \le 1 \qquad (2a)$$

$$[\phi_\xi] + k[\phi_\tau] = 0 \quad ; \eta = 0,\ \xi = 1 \qquad (2b)$$

The wake, which is represented as a slit downstream of the airfoil trailing edge, has the boundary condition

$$[\phi_\xi] + k[\phi_\tau] = 0 \quad ; \eta = 0,\ \xi > 1 \qquad (3)$$

Numerical solutions of Eq. (1) were obtained using the alternating-direction implicit algorithm of Rizzetta and Chin.[18] The Rizzetta-Chin algorithm is similar to that used in the LTRAN2 code[12] with the addition of a three-time-level representation of the $\frac{k^2 M_\infty^2}{\delta^{2/3}} \phi_{\tau\tau}$ term on the η-sweep.

The code XTRAN2L was developed by incorporating the Rizzetta-Chin algorithm into the low/moderate frequency code HYTRAN2.[16] The HYTRAN2 program is a modified version of the LTRAN2-NLR code which was derived from the LTRAN2 program. The TSP equation and boundary conditions in the LTRAN2 program are low frequency approximations and do not include the time derivative terms. The HYTRAN2 code (and LTRAN2-NLR) is a moderate frequency version and includes the time derivative terms in the boundary conditions. Since XTRAN2L solves the complete TSP equation, it has no restrictions on the allowable values of k (LTRAN2 begins to fail at $k \approx 0.075$, and HYTRAN2 is valid for $k < 0.4$).

Engquist and Majda[25] developed far-field radiation boundary conditions for the low frequency equation (without the $\frac{k^2 M_\infty^2}{\delta^{2/3}} \phi_{\tau\tau}$ term) which were incorporated into LTRAN2 by Kwak.[26] Those boundary conditions reduced the disturbances reflecting from the computational boundaries. Since the boundary conditions of ref. 25 are applicable only to the low frequency equation, far-field radiation conditions consistent with Eq. (1) have been developed and implemented into XTRAN2L. These conditions allow the use of smaller grids while significantly reducing reflections from the grid boundaries. Far-field radiation boundary conditions were used in analyzing the XTRAN2L default grid while reflecting far-field boundary conditions described in ref. 14 were used in analyzing all the other grids.

Pulse Technique

In order to determine the accuracy of results obtained using a particular grid, the linear unsteady aerodynamic forces on a flat plate are calculated for a wide range of reduced frequencies. The forces are compared to the known exact theoretical values to determine the grid characteristics. Typically, unsteady aerodynamic forces are determined by calculating several cycles of forced harmonic oscillations with the last cycle providing the estimate of the forces. Alternatively, the estimates may be obtained from Fourier transformation of the response to a step change in a given mode of motion.[13] The harmonic oscillation technique is costly since calculations may be required for 5-10 reduced frequencies. In contrast, the indicial response approach can be inaccurate for finite difference solutions of Eq. (1). The discontinuous initial condition caused by a step function can only be roughly approximated and thus an error in the calculation of the airfoil loads is introduced and the resulting forces can be inaccurate. It was suggested in ref. 27 that the use of a smooth pulse would alleviate this problem. A different pulse from that of ref. 27 is used in this study. It is a pulse in pitch about the quarter-chord defined by

$$\alpha = \alpha_0 + \frac{\pi}{360} e^{-(\tau-\tau_c)^2}$$

where

$$\tau_c = 57.5\Delta\tau$$

This gives a pulse with a maximum amplitude of one-half degree with a smooth transition from a steady-state condition to the pulse. The calculation is carried out for a total of 1024 time steps to assure a return of the flow field to the steady-state condition.

Fast Fourier transforms (FFTs) of the lift coefficient, the moment coefficient about the quarter-chord, and the angle of attack time histories are then calculated. The lift and moment coefficient FFTs are divided by the α FFT to obtain the frequency response functions for c_{ℓ_α} and c_{m_α} as shown in Fig. 1. For most cases the unsteady lift and moment show the same grid characteristics, and only the calculated lift is shown. The pulse was designed to have sufficient magnitude to obtain reasonable results for frequencies up to k = 2.0. The use of the pulse and transfer function technique gives considerable detail in the frequency domain with a significant reduction in cost over calculating discrete oscillations.

The linear analysis is performed for a flat plate at $M_\infty = 0.850$, $\Delta\tau = \pi/12.80$, $\alpha_0 = 0.$ rad. and $V_\infty/c = 100.0$. The resulting forces are compared to the exact forces calculated by a two-dimensional subsonic kernel function aerodynamics program described in ref. 28. The comparison gives an excellent indication of the effect of the grid for a wide range of reduced frequencies. The analysis is also performed on a 6% thick parabolic arc airfoil at the same conditions as the flat plate to demonstrate the non-linear transonic effects. For lifting conditions, the steady-state and unsteady algorithms converge to slightly different solutions, so before the pulse is applied the airfoil is held fixed and the unsteady solution is calculated for 1024 time steps to obtain a consistent initial condition. This ensures that the lift and moment after the pulse return to the initial values and eliminates low frequency errors which might be introduced in the FFT results.

Grids Analyzed

Five computational grids are evaluated using the pulse-transfer function technique. Three are the default grids from currently used TSP finite difference programs; the LTRAN2-NLR program,[14] the LTRAN2-HI program,[15] and the x,z grid of the XTRAN3S program.[23] In addition, two grids designed to improve the accuracy of the calculated forces are analyzed.

The default grid of the LTRAN2-NLR program consists of 99 x 79 points in x,z, and the grid coordinates for the flat plate case are listed in Table 1. Figure 2 illustrates the LTRAN2-NLR grid in the region around the flat plate with a typical airfoil drawn to illustrate the airfoil location. The physical grid for the flat plate case extends from -1034c to 856c in x and ∓3860c in z with 33 grid points on the airfoil. Since the far-field boundary conditions of the LTRAN2-NLR program are reflecting, the physical mesh extent is several thousand chordlengths in both directions. The TSP equation is solved in a transformed coordinate system, so the physical grid is mapped into computational coordinates. In LTRAN2-NLR the computational space ξ,η grid is identical for all cases and related to the physical x,z grid by

$$x = \xi$$
$$z = \frac{\eta}{\{\delta M_\infty^2(\gamma^*+1)\}^{1/3}}$$

The physical x grid is fixed and the z grid varies with Mach number, thickness ratio, and ratio of specific heats. For the flat plate airfoil a value of $\delta = 0.005$ is used.

TABLE 1. LTRAN2-NLR DEFAULT GRID FOR $M_\infty = 0.850$, $\delta = 0.005$

INDEX	x	z
1	-1033.53047	-3860.13477
2	-749.90681	-2503.05607
3	-544.02252	-1649.54460
4	-394.58328	-1112.74704
5	-286.12668	-775.13626
6	-207.42501	-562.80681
7	-150.32551	-429.26193
8	-108.90823	-335.50205
9	-78.87451	-262.01548
10	-57.10299	-204.43719
11	-41.32715	-159.34467
12	-29.90121	-124.04846
13	-21.63011	-96.43506
14	-15.64610	-74.85272
15	-11.31906	-57.99242
16	-8.19147	-44.84499
17	-5.93108	-34.60124
18	-4.29666	-26.62805
19	-3.11304	-20.44467
20	-2.25301	-15.64648
21	-1.62421	-11.94312
22	-1.15958	-9.08705
23	-.81673	-6.89740
24	-.56674	-5.21708
25	-.38898	-3.94327
26	-.26502	-2.97364
27	-.17974	-2.24154
28	-.12149	-1.69079
29	-.08171	-1.27761
30	-.05433	-.96725
31	-.03517	-.73306
32	-.02142	-.55312
33	-.01123	-.41080
34	-.00330	-.29403
35	.00330	-.19140
36	.00929	-.11662
37	.01534	-.06997
38	.02204	-.04046
39	.03003	-.01571
40	.03998	0.00000
41	.05260	.01571
42	.06871	.04046
43	.08916	.06997
44	.11478	.11662
45	.14619	.19140
46	.18359	.29403

TABLE 1. - CONTINUED

INDEX	x	z
47	.22663	.41080
48	.27436	.55312
49	.32552	.73306
50	.37877	.96725
51	.43295	1.27761
52	.48720	1.69079
53	.54078	2.24154
54	.59298	2.97364
55	.64314	3.94327
56	.69075	5.21708
57	.73559	6.89740
58	.77770	9.08705
59	.81705	11.94312
60	.85334	15.64648
61	.88595	20.44467
62	.91425	26.62805
63	.93798	34.60124
64	.95746	44.84499
65	.97351	57.99242
66	.98726	74.85272
67	1.00000	96.43506
68	1.01306	124.04846
69	1.02785	159.34467
70	1.04593	204.43719
71	1.06923	262.01548
72	1.10047	335.50205
73	1.14381	429.26193
74	1.20541	562.80681
75	1.29376	775.13626
76	1.41949	1112.74704
77	1.59483	1649.54460
78	1.83264	2503.05607
79	2.15087	3860.13477
80	2.58083	
81	3.17250	
82	3.99545	
83	5.14646	
84	6.76021	
85	9.02411	
86	12.19890	
87	16.64743	
88	22.87456	
89	31.58279	
90	43.74965	
91	60.73530	
92	84.43235	
93	117.47431	

TABLE 1. - CONTINUED

INDEX	x	z
94	163.52559	
95	227.68509	
96	317.04773	
97	441.48577	
98	614.73612	
99	855.91313	

The LTRAN2-HI default grid consists of 113 x 97 points in the x,z plane and is listed in Table 2 and illustrated in Fig. 3. For the flat plate case the physical extent of the grid is ∓200c in x and ∓2327c in z with 48 grid points on the airfoil. The far-field boundary conditions in the program are also reflecting so the physical extent is quite large. The computational ξ,η grid in LTRAN2-HI is related to physical x,z space by

$$x = \xi$$

$$z = \frac{\eta}{\delta^{1/3}}$$

The x grid is again fixed while the z grid depends only upon the thickness ratio.

TABLE 2. LTRAN2-HI DEFAULT GRID FOR $\delta = 0.005$

INDEX	x	z
1	-200.00000	-2326.50510
2	-132.08390	-1694.05485
3	-87.24290	-1240.86615
4	-57.65660	-914.37169
5	-38.15274	-677.87267
6	-25.31051	-505.62532
7	-16.86743	-379.48372
8	-11.32718	-286.59564
9	-7.70010	-217.81429
10	-5.33166	-166.59850
11	-3.78896	-128.24781
12	-2.78570	-99.36814
13	-2.13252	-77.49680
14	-1.70418	-60.83830
15	-1.41785	-48.07719
16	-1.21875	-38.24505
17	-1.07500	-30.62553

TABLE 2. - CONTINUED.

INDEX	x	z
18	-.95000	-24.68612
19	-.82500	-20.02908
20	-.70000	-16.35590
21	-.57500	-13.44147
22	-.45625	-11.11518
23	-.35000	-9.24715
24	-.25625	-7.73799
25	-.18125	-6.51133
26	-.12500	-5.50815
27	-.08188	-4.68267
28	-.05375	-3.99918
29	-.03625	-3.42973
30	-.02375	-2.95229
31	-.01500	-2.54946
32	-.00813	-2.20742
33	-.00250	-1.91512
34	.00250	-1.66372
35	.00750	-1.44609
36	.01250	-1.25646
37	.01750	-1.09014
38	.02250	-.94330
39	.02750	-.81278
40	.03250	-.69600
41	.03813	-.59080
42	.04563	-.49539
43	.05500	-.40827
44	.06500	-.32815
45	.07500	-.25398
46	.08563	-.18482
47	.09875	-.11988
48	.11703	-.05848
49	.14204	0.00000
50	.17188	.05848
51	.20313	.11988
52	.23438	.18482
53	.26563	.25398
54	.29688	.32815
55	.32813	.40827
56	.35938	.49539
57	.39063	.59080
58	.42188	.69600
59	.45313	.81278
60	.48438	.94330
61	.51563	1.09014
62	.54688	1.25646
63	.57813	1.44609
64	.60938	1.66372
65	.64063	1.91512

TABLE 2. - CONTINUED

INDEX	x	z
66	.67188	2.20742
67	.70313	2.54946
68	.73438	2.95229
69	.76563	3.42973
70	.79688	3.99918
71	.82813	4.68267
72	.85797	5.50815
73	.88235	6.51133
74	.90000	7.73799
75	.91500	9.24715
76	.93000	11.11518
77	.94500	13.44147
78	.96000	16.35590
79	.97500	20.02908
80	.98875	24.68612
81	1.00000	30.62553
82	1.01125	38.24505
83	1.02750	48.07719
84	1.05375	60.83830
85	1.09500	77.49680
86	1.15375	99.36814
87	1.22500	128.24781
88	1.30625	166.59850
89	1.40000	217.81429
90	1.50625	286.59564
91	1.62500	379.48372
92	1.75000	505.62532
93	1.87500	677.87267
94	2.01875	914.37169
95	2.22799	1240.86615
96	2.51972	1694.05485
97	2.92056	2326.50510
98	3.46671	
99	4.20744	
100	5.20975	
101	6.56481	
102	8.39662	
103	10.87389	
104	14.22615	
105	18.76560	
106	24.91700	
107	33.25817	
108	44.57519	
109	59.93742	
110	80.79963	
111	109.14088	
112	147.65347	
113	200.00000	

The grid implemented in XTRAN2L is designed to improve the accuracy of the calculated forces for two-dimensional flow problems. It is 80 x 61 points in x,z and is listed in Table 3 and shown in Fig. 4. The physical grid extends ∓20c in x and ∓25c in z with 51 grid points lying on the airfoil. The physical extent of the grid is fixed and is related to the computational grid in XTRAN2L by

$$x = \xi$$

$$z = \frac{\eta}{\{\delta M_\infty^2(\gamma^*+1)\}^{1/3}}$$

The computational ξ grid is fixed for all problems while the η grid will vary depending upon M_∞, δ, and γ^*. The XTRAN2L grid takes advantage of the far-field radiation boundary conditions incorporated in the program by reducing the physical extent covered. Reducing the area covered by the grid allows the number of points in the grid to be decreased, permits the inclusion of more grid points on the airfoil, and reduces the computational cost. The XTRAN2L grid consists of a smooth stretching in z and in x upstream and downstream of the airfoil.

On the airfoil, the LTRAN2-NLR and LTRAN2-HI programs concentrate grid points near the leading and trailing edges because of rapid changes in pressure near the airfoil edges. The grid spacing on the airfoil is maximum near the middle of the airfoil. Yet the change in pressure across a shock is of the same magnitude as the change in pressure near the airfoil edges so the grid spacing around the shock should also be fine. Unfortunately, the shock very likely will occur in the region where both grids have relatively large grid spacing, causing reduced shock resolution.

Since the pressure gradient across a shock may be greater than that near the trailing edge, the XTRAN2L grid has no special concentration of points near the airfoil trailing edge. The XTRAN2L grid points on the airfoil were equally spaced to allow a better shock definition for any position and transient motion. Keyfitz, Melnick and Grossman[29] show that the grid spacing near a blunt leading edge is important in TSP codes and the best results may be obtained for a medium mesh spacing. Thus no fine grid spacing is used near the leading edge but a grid point was added near the nose to aid in defining a blunt airfoil.

TABLE 3. XTRAN2L DEFAULT GRID

INDEX	x	z
1	-20.00000	-25.00000
2	-16.30961	-23.36111
3	-13.10054	-21.77778
4	-10.33987	-20.25000
5	-7.99453	-18.77778
6	-6.03136	-17.36111
7	-4.41705	-16.00000

TABLE 3. CONTINUED

INDEX	x	z
8	-3.11817	-14.69444
9	-2.10110	-13.44444
10	-1.33204	-12.25000
11	-.77699	-11.11111
12	-.40170	-10.02778
13	-.17160	-9.00000
14	-.05175	-8.02778
15	-.00667	-7.11111
16	.00667	-6.25000
17	.02000	-5.44444
18	.04000	-4.69444
19	.06000	-4.00000
20	.08000	-3.36111
21	.10000	-2.77778
22	.12000	-2.25000
23	.14000	-1.77778
24	.16000	-1.36111
25	.18000	-1.00000
26	.20000	-.69444
27	.22000	-.44444
28	.24000	-.25000
29	.26000	-.11111
30	.28000	-.02778
31	.30000	0.00000
32	.32000	.02778
33	.34000	.11111
34	.36000	.25000
35	.38000	.44444
36	.40000	.69444
37	.42000	1.00000
38	.44000	1.36111
39	.46000	1.77778
40	.48000	2.25000
41	.50000	2.77778
42	.52000	3.36111
43	.54000	4.00000
44	.56000	4.69444
45	.58000	5.44444
46	.60000	6.25000
47	.62000	7.11111
48	.64000	8.02778
49	.66000	9.00000
50	.68000	10.02778
51	.70000	11.11111
52	.72000	12.25000
53	.74000	13.44444
54	.76000	14.69444
55	.78000	16.00000
56	.80000	17.36111

TABLE 3. CONTINUED

INDEX	x	z
57	.82000	18.77778
58	.84000	20.25000
59	.86000	21.77778
60	.88000	23.36111
61	.90000	25.00000
62	.92000	
63	.94000	
64	.96000	
65	.98000	
66	1.00000	
67	1.02000	
68	1.12274	
69	1.35473	
70	1.75323	
71	2.35080	
72	3.17695	
73	4.25898	
74	5.62249	
75	7.29170	
76	9.28970	
77	11.63860	
78	14.35968	
79	17.47352	
80	21.00000	

The XTRAN3S program is a 3-dimensional TSP finite difference code. For analysis with the XTRAN2L program the default x,z grid defined at the root chord is studied. The grid coordinates are listed in Table 4 and the near-field grid is shown in Fig. 5. The physical extent of the grid is from -15c to 27c in x and ∓13c in z with 39 grid points on the airfoil. The XTRAN3S program has reflecting far-field boundary conditions and the grid is limited to 60 x 40 points in the x,z plane. This limitation results in the boundaries being defined very close to the airfoil as compared to the previously described grids. The physical grid is invariant and related to the XTRAN3S computational grid by

$$x - x_{LE} = \xi$$

$$z = \eta$$

where x_{LE} is the leading edge location (=0 at root chord). The computational and physical grids at the root chord are identical and are problem independent. For analysis with XTRAN2L a grid row at z = 0 was added to the XTRAN3S default z grid because the XTRAN2L program requires a grid row at z = 0 while the XTRAN3S program does not.

TABLE 4. XTRAN3S DEFAULT GRID

INDEX	x	z
1	-15.37500	-13.03750
2	-7.69250	-6.63750
3	-3.85000	-3.43750
4	-1.92750	-1.83750
5	-.96500	-1.03750
6	-.48250	-.63750
7	-.24000	-.43750
8	-.11750	-.33750
9	-.05500	-.28750
10	-.02250	-.26250
11	-.00500	-.23750
12	.00500	-.21250
13	.01500	-.18750
14	.02500	-.16250
15	.03500	-.13750
16	.04500	-.11250
17	.06000	-.08750
18	.08000	-.06250
19	.10000	-.03750
20	.13000	-.01250
21	.16000	0.00000
22	.19000	.01250
23	.22000	.03750
24	.25000	.06250
25	.28000	.08750
26	.31000	.11250
27	.34000	.13750
28	.37000	.16250
29	.40000	.18750
30	.43000	.21250
31	.46000	.23750
32	.49000	.26250
33	.52000	.28750
34	.55000	.33750
35	.58000	.43750
36	.61000	.63750
37	.64000	1.03750
38	.67000	1.83750
39	.70000	3.43750
40	.73000	6.63750
41	.76000	13.03750
42	.79000	
43	.82000	
44	.85000	
45	.88000	
46	.91000	
47	.93500	
48	.96000	
49	.98000	

TABLE 4. - CONTINUED

INDEX	x	z
50	1.00000	
51	1.02500	
52	1.07500	
53	1.17500	
54	1.37500	
55	1.77500	
56	2.57500	
57	4.17500	
58	7.37500	
59	13.77500	
60	26.57500	

A revised XTRAN3S x,z grid was designed to improve the accuracy of the calculated forces and is listed in Table 5 and shown in Fig. 6. The physical extent of the grid is ∓20c in x and ∓25c in z with 39 points lying on the airfoil. The grid also is problem-independent and has a z = 0 grid line added for the two-dimensional analysis. The grid was optimized for the available size of 60 x 40 points in the x,z plane. To minimize the reflections from the z boundary, the extent covered by the z grid is increased to ∓25 chordlengths. A smooth stretching is used in z and in x upstream and downstream of the airfoil. The points on the airfoil are equi-spaced with an additional point near the leading edge for better nose definition.

TABLE 5. REVISED XTRAN3S GRID

INDEX	x	z
1	-20.00000	-25.00000
2	-14.70824	-22.50164
3	-10.47170	-20.13478
4	-7.16272	-17.89941
5	-4.65677	-15.79553
6	-2.83281	-13.82314
7	-1.57362	-11.98225
8	-.76633	-10.27285
9	-.30308	-8.69494
10	-.08199	-7.24852
11	-.00877	-5.93360
12	.00877	-4.75016
13	.02632	-3.69822
14	.05263	-2.77778
15	.07895	-1.98882
16	.10526	-1.33136
17	.13158	-.80539
18	.15789	-.41091
19	.18421	-.14793
20	.21053	-.01644
21	.23684	0.00000

TABLE 5. - CONTINUED.

INDEX	x	z
22	.26316	.01644
23	.28947	.14793
24	.31579	.41091
25	.34211	.80539
26	.36842	1.33136
27	.39474	1.98882
28	.42105	2.77778
29	.44737	3.69822
30	.47368	4.75016
31	.50000	5.93360
32	.52632	7.24852
33	.55263	8.69494
34	.57895	10.27285
35	.60526	11.98225
36	.63158	13.82314
37	.65789	15.79553
38	.68421	17.89941
39	.71053	20.13478
40	.73684	22.50164
41	.76316	25.00000
42	.78947	
44	.84211	
45	.86842	
46	.89474	
47	.92105	
48	.94737	
49	.97368	
50	1.00000	
51	1.02632	
52	1.19383	
53	1.62332	
54	2.42771	
55	3.71531	
56	5.59119	
57	8.15791	
58	11.51599	
59	15.76424	
60	21.00000	

RESULTS AND DISCUSSION

Linear Flat Plate Analysis

LTRAN2-NLR GRID

The first grid analyzed using the pulse-transfer function technique is the LTRAN2-NLR grid. The grid was analyzed using the reflecting far-field boundary conditions used in the LTRAN2-NLR program. Figure 7 presents c_{ℓ_α} versus reduced frequency for this grid at $M_\infty = 0.850$ and for the corresponding exact values obtained from a kernel function solution. In addition to obtaining the unsteady forces for the complete TSP equation on this grid, the unsteady forces are also calculated for the low frequency equation and boundary conditions[14] and are included to show the effect of adding the time derivative terms to the equations.

Both finite difference solutions exhibit spurious oscillations in the calculated unsteady forces. The complete equation solution exhibits slightly larger oscillations than the low frequency results. The low frequency solution deviates from the complete and exact solutions for reduced frequencies greater than 0.075. Several modifications of the grid were conducted to determine the cause of this oscillation. The resulting unsteady forces are very insensitive to the x grid extent and spacing off of the airfoil while the z grid extent and spacing are very critical. For the physical time span covered in the flat plate cases, the maximum distance from which disturbances can be reflected back to the airfoil is 41c in x and 77c in z. The x grid boundaries were moved to within 4 chordlengths of the airfoil before any noticeable change occured in the unsteady forces, while changes were noticeable when the z boundaries came within 75 chordlengths of the airfoil.

The oscillations are due to internal numerical reflections in the grid caused by stretching too rapidly in the z direction and were traced to the grid spacing at approximately 9 chordlengths from the airfoil. The disturbances from the airfoil due to the pulse are unable to propagate accurately between the grid points which are approximately 2 chordlengths apart and are partially reflected back to the airfoil. The reflected disturbances cause oscillations in the force time histories as shown in Fig. 1 and result in the oscillations in the force frequency response functions. Adding the time derivative terms by going from the low frequency to the complete equation causes the oscillations to increase in magnitude.

As the reduced frequency increases, the LTRAN2-NLR forces begin to deviate from the exact values. This is not due to the grid but is caused by using too large a time step. The calculated forces can be brought into closer agreement with the kernel function values at the higher reduced frequencies by decreasing the time step. To maintain accuracy at the low reduced frequencies, the number of steps should be increased such that the total time the solution spans remains constant. The phenomenon of decreasing agreement with the exact kernel function values for increasing reduced frequency for the pulse-generated forces occurs for all cases in this paper since they all were run for the identical number of time steps and total time.

LTRAN2-HI

Results from the LTRAN2-HI grid analyzed using reflecting far-field boundary conditions are shown in Fig. 8. This grid is very similar to the LTRAN2-NLR grid and shows the same oscillations in unsteady forces. Internal grid reflections affect the forces for reduced frequencies above 0.20. The magnitude and extent of the oscillations in the forces are not as severe for the LTRAN2-HI grid as for the LTRAN2-NLR grid. This is due to the slightly finer spacing of the LTRAN2-HI grid around 9 chordlengths away in z than that found in the LTRAN2-NLR grid.

XTRAN2L Grid

The results for the XTRAN2L grid are shown in Figs. 9 and 10. In order to see the effect of the radiation boundary conditions, the grid was first analyzed with the reflecting far-field boundary conditions used for the LTRAN2-NLR and LTRAN2-HI grids (Fig. 9). The calculated forces agree quite well with the kernel function values except for the oscillations near $k = 0.08$. These oscillations are due to reflections of disturbance from the z boundary at ∓ 25 chordlengths from the wing. Including the radiation far-field boundary conditions alleviates the oscillations as shown in Fig. 10.

In addition to giving more accurate forces, the XTRAN2L grid gives a considerable savings in computational cost due to the fewer number of grid points used. The computer time required to calculate forces using this grid is 34% less than the time taken for the LTRAN2-NLR grid and 53% less than that for the LTRAN2-HI grid. The program size is also reduced by 15% and 28% as compared to LTRAN2-NLR and LTRAN2-HI programs respectively.

XTRAN3S Default Grid

The forces calculated for the default XTRAN3S root chord x,z grid using reflecting far-field boundary conditions are shown in Fig. 11. Very poor agreement with the exact values is exhibited. The XTRAN3S grid exhibits both internal and boundary reflections. For $k < 0.3$ the oscillations are due to reflections from the z boundary and for $k > 0.3$ are caused by internal grid reflections from approximately 3 chordlengths above and below the airfoil.

XTRAN3S Revised Grid

The results for the revised XTRAN3S root chord x,z grid using reflecting far-field boundary conditions are shown in Fig. 12. The revised grid exhibits much better agreement with the exact values than the original grid. The amplitude and frequency of the boundary reflections are decreased due to the larger extent of the grid in z. The effects of internal grid reflections are eliminated for $k < 0.50$ and minimized for $k > 0.50$. Neither the boundary nor the internal reflections can be eliminated completely due to the program size restrictions and reflecting boundary conditions. The results represent a compromise grid designed to optimize accuracy for $k < 0.50$, which is the range of interest for flutter analysis.

6% Parabolic Arc Analysis

To investigate non-linear transonic effects, calculations were made for a six percent thick parabolic arc airfoil using the LTRAN2-NLR, LTRAN2-HI, and XTRAN2L grids. The LTRAN2-NLR and LTRAN2-HI grids were analyzed using reflecting far-field boundary conditions while the XTRAN2L grid used the radiation boundary conditions. The forces calculated using the XTRAN2L grid at $M_\infty = 0.850$ are shown in Fig. 13. To verify the accuracy of the pulse-transfer function technique for this non-linear case, harmonic oscillatory solutions were obtained for discrete reduced frequencies. Figure 13 demonstrates that the harmonic and pulse unsteady forces agree well with each other for moderate reduced frequencies and verifies that for this case, the unsteady forces may be treated as locally linear. As demonstrated in the linear flat plate cases, the agreement becomes worse with increasing reduced frequency. The agreement can be improved by decreasing the time step for the pulse case.

The forces for the three grids are compared in Figs. 14 and 15. Figure 14 demonstrates that all three grids predict values of c_{ℓ_α} that are close to one another. The LTRAN2-NLR and LTRAN2-HI grids cause internal reflections as in the linear flat plate case. The magnitude of the oscillations for this non-linear case are smaller than for the corresponding linear cases shown in Figs. 7 and 8. The pitching moments shown in Fig. 15 also exhibit the internal reflections and, in addition, demonstrate a difference in the value of c_{m_α} between the three grids.

To illustrate the source of the difference exhibited in the values of c_{m_α}, the steady-state pressure distributions of the airfoil for each grid are shown in Fig. 16. As the grid spacing on the airfoil becomes finer, the shock definition becomes better and the shock strength increases. As the shock strength increases, the lift is not changed to any measureable degree but the moment increases. Grid spacing along the airfoil can thus be very important to the shock definition and hence the resulting forces.

CONCLUDING REMARKS

A pulse-transfer function method for calculating unsteady aerodynamic forces for a wide range of reduced frequencies has been implemented in an unsteady transonic small perturbation finite difference code. The forces were determined for a two-dimensional linear flat plate and compared to exact theoretical values to evaluate the grid. The LTRAN2-NLR grid exhibited internal reflections which can be eliminated by improving the z stretching. The LTRAN2-HI grid was shown to be superior to the LTRAN2-NLR grid but to still have internal reflections. The addition of far-field radiation boundary conditions for the complete equation permitted a decrease in grid size and resulted in a 34% savings in computing time while eliminating the internal reflections. The unsteady forces calculated with the XTRAN3S grid were shown to be inaccurate due to boundary and internal numerical reflections. A redesigned grid utilizing the same total number of points but spanning a larger extent and having an improved stretching in z was shown to increase the accuracy.

Calculations for a 6% thick parabolic arc airfoil demonstrated that grid problems encountered for the linear flat plate airfoil also occur for non-linear cases. The pulse-transfer function technique was shown to work for a non-linear case, indicating that the unsteady forces can be treated as locally linear. In addition, the grid spacing was shown to influence the shock definition which in turn affects the unsteady pitching moment. Finer grid spacing on the airfoil was used to adequately capture shock definition and motion.

REFERENCES

1. Smith, R. E., ed: Numerical Grid Generation Techniques. NASA CP-2166, 1980.

2. Steger, J. L. and Bailey, H. E.: Calculation of Transonic Aileron Buzz. AIAA Journal, vol. 18, no. 3, March 1980, pp. 249-255.

3. Magnus, R. and Yoshihara, H.: Unsteady Flows over an Airfoil. AIAA Journal, vol. 13, no. 12, Dec. 1975, pp. 1622-1628.

4. Magnus, R. J.: Calculation of Some Unsteady Transonic Flows About the NACA 64A006 and 64A010 Airfoils. AFFDL-TR-77-46, U. S. Air Force, July 1977.

5. Chyu, W. J. and Davis, S. S.: Calculation of Unsteady Transonic Flow Over an Arbitrary Airfoil. AIAA Paper 79-1554, July 1979.

6. Isogai, Koji: Calculation of Unsteady Transonic Flow over Oscillating Airfoils Using the Full Potential Equation. AIAA/ASME 18th Structures, Structural Dynamics and Materials Conference, Vol. B (San Diego, California), March 1977, pp. 245-256.

7. Chipman, R. and Jameson, A.: Fully Conservative Numerical Solutions for Unsteady Irrotational Transonic Flow About Airfoils. AIAA Paper 79-1555, July 1979.

8. Chipman, R. and Jameson, A.: An Alternating-Direction-Implicit Algorithm for Unsteady Potential Flow. AIAA Paper 81-0329, 1981.

9. Chang, I-Chung: Unsteady Transonic Flow Past Airfoils in Rigid Body Motion. Courant Inst. of Math Sci., NYU Res. and Dev. Rept. DOE/ER/03077-170, March 1981.

10. Goorjian, P. M.: Implicit Computation of Unsteady Transonic Flow Governed by the Full Potential Equation in Conservation Form. AIAA Paper 80-150, 1980.

11. Bennett, R. M. and Bland, S. R.: An Exploratory Study of a Finite Difference Method for Calculating Unsteady Potential Flow. NASA TM 80105, June 1979.

12. Ballhaus, W. F. and Goorjian, P. M.: Implicit Finite-Difference Computation of Unsteady Transonic Flows About Airfoils. AIAA Journal, vol. 15, no. 12, Dec. 1977, pp. 1728-1735.

13. Ballhaus, W. F. and Goorjian, P. M.: Computation of Unsteady Transonic Flows by the Indicial Method. AIAA Journal, vol. 16, no. 2, Feb. 1978, pp. 117-124.

14. Huizing, G. H. and van der Vooren, J.: Users Manual for LTRAN2-NLR; A Programme for the Calculation of Inviscid Transonic Flow About Thin Airfoils in Moderately Slow Unsteady Motion. Memorandum W-79-003, NLR, June 1979.

15. Hessenius, K. A. and Goorjian, P. M.: Validation of LTRAN2-HI by Comparison with Unsteady Transonic Experiment. AIAA Journal, vol. 20, no. 5, May 1982, pp. 731-732.

16. Edwards, J. W.; Bennett, R. M.; Whitlow, W., Jr.; and Seidel, D. A.: Time-Marching Transonic Flutter Solutions Including Angle-of-Attack Effects. AIAA Paper 82-0685, May 1982.

17. Yang, T. Y. and Chen, C. H.: Transonic Flutter and Response Analyses of Two 3-Degree-of-Freedom Airfoils. Journal of Aircraft, vol. 19, no. 10, Oct. 1982, pp. 875-884.

18. Rizzetta, D. P. and Chin, W. C.: Effect of Frequency in Unsteady Transonic Flow. AIAA Journal, vol. 17, no. 7, July 1979, pp. 779-781.

19. Rizzetta, D. P. and Yoshihara, H.: Computation of the Pitching Oscillation of an NACA 64A010 Airfoil in the Small Disturbance Limit. AIAA Paper 80-0128, 1980.

20. Isogai, K.: Numerical Study of Transonic Flutter of a Two-Dimensional Airfoil. NAL TR-617T, National Aerospace Inst., Tokyo, Japan, July 1980.

21. Weatherill, W. H.; Sebastian, J. D.; and Ehlers, F. E.: The Practical Application of a Finite Difference Method for Analyzing Transonic Flow over Oscillating Airfoils and Wings. NASA CR-2933, 1978.

22. Ehlers, F. E. and Weatherill, W. H.: A Harmonic Analysis Method for Unsteady Transonic Flow and Its Application to the Flutter of Airfoils. NASA CR-3537, May 1982.

23. Borland, C. J. and Rizzetta, D. P.: Nonlinear Transonic Flutter Analysis. AIAA Journal, vol. 20, no. 11, Nov. 1982, pp. 1606-1615.

24. Isogai, K.: Transonic Dip Mechanism of Flutter of a Sweptback Wing: Part II. AIAA Journal, vol. 19, no. 9, Sept. 1981, pp. 1240-1241.

25. Engquist, B. and Majda, A.: Numerical Radiation Boundary Conditions for Unsteady Transonic Flow. Journal of Computational Physics, vol. 40, 1981, pp. 91-103.

26. Kwak, D.: Non-reflecting Far-Field Boundary Conditons for Unsteady Transonic Flow Computation. AIAA Paper 80-1393, July 1980.

27. Davies, D. E. and Salmond, D. J.: Indicial Approach to Harmonic Perturbations in Transonic Flow. AIAA Journal, vol. 18, no. 8, August 1980, pp. 1012-1014.

28. Bland, S. R.: Development of Low-Frequency Kernel-Function Aerodynamics for Comparison with Time-Dependent Finite-Difference Methods. NASA TM-83283, May 1982.

29. Keyfitz, B. L.; Melnik, R. E.; and Grossman, B.: Analytic and Numerical Solutions of the Transonic Small-Distance Equation in the Vicinity of a Blunt Leading Edge. AIAA Paper 77-676, June 1977.

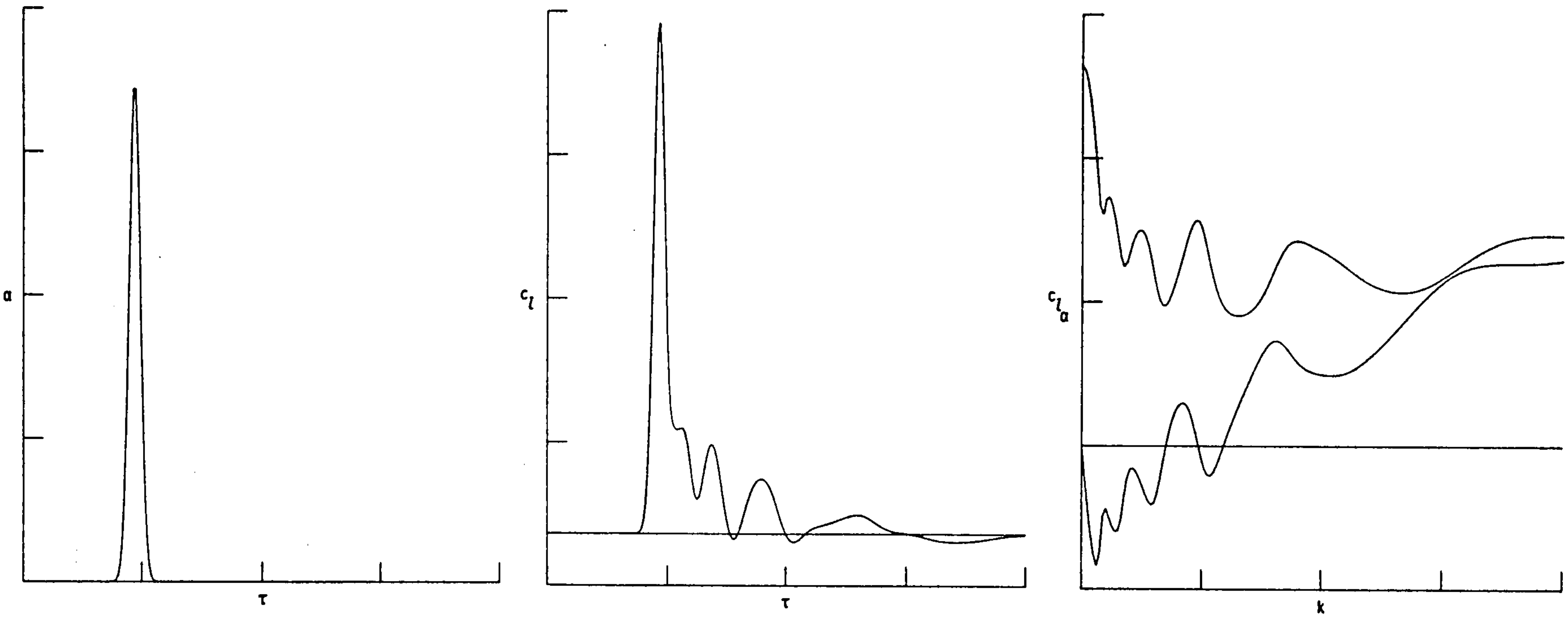

(a) Pulse input (b) Force output (c) Unsteady forces

Fig. 1 Pulse-transfer function analysis for unsteady aerodynamic forces.

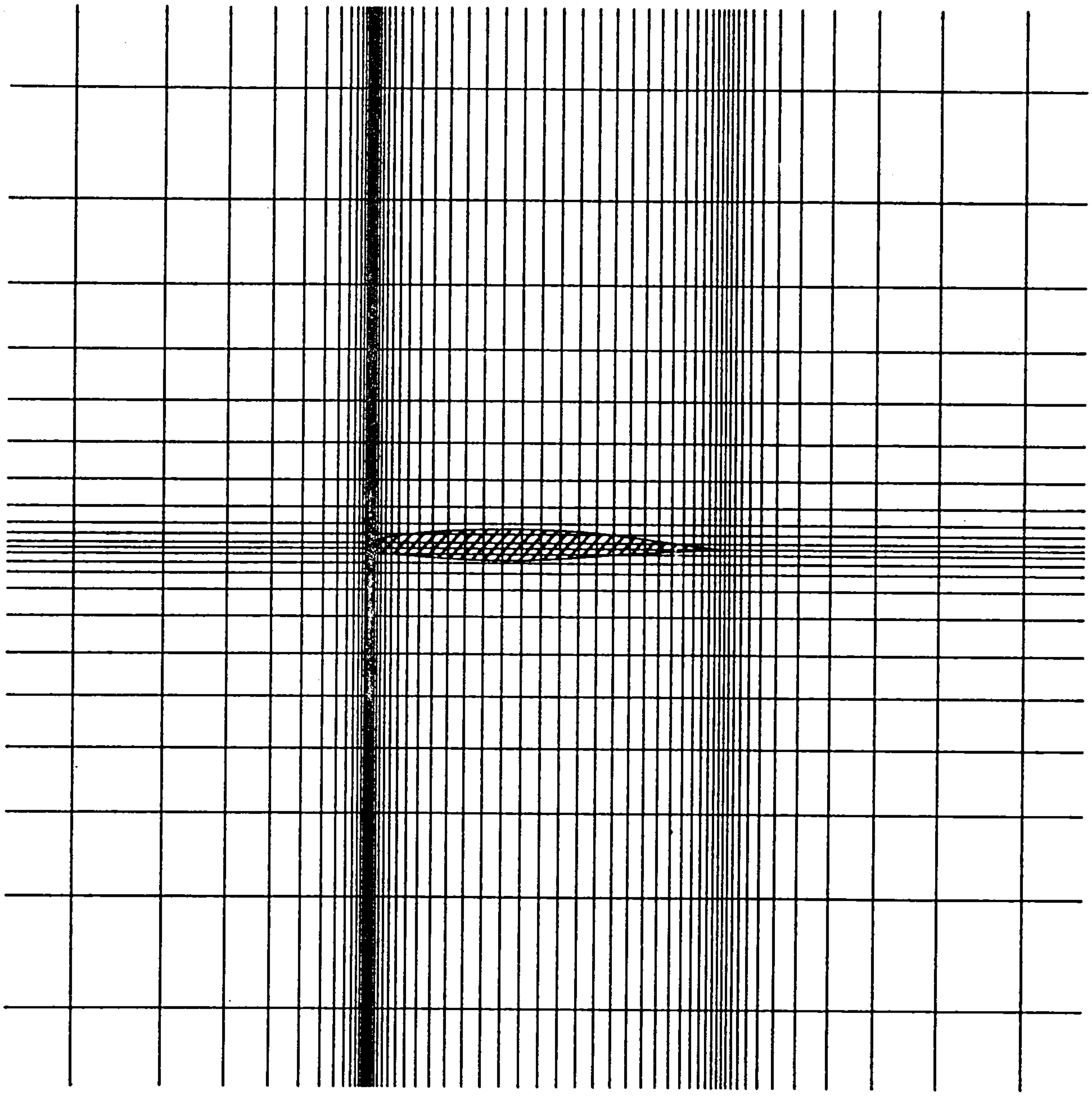

Fig. 2 LTRAN2-NLR default grid near the airfoil for $M_\infty = 0.850$, $\delta = 0.005$.

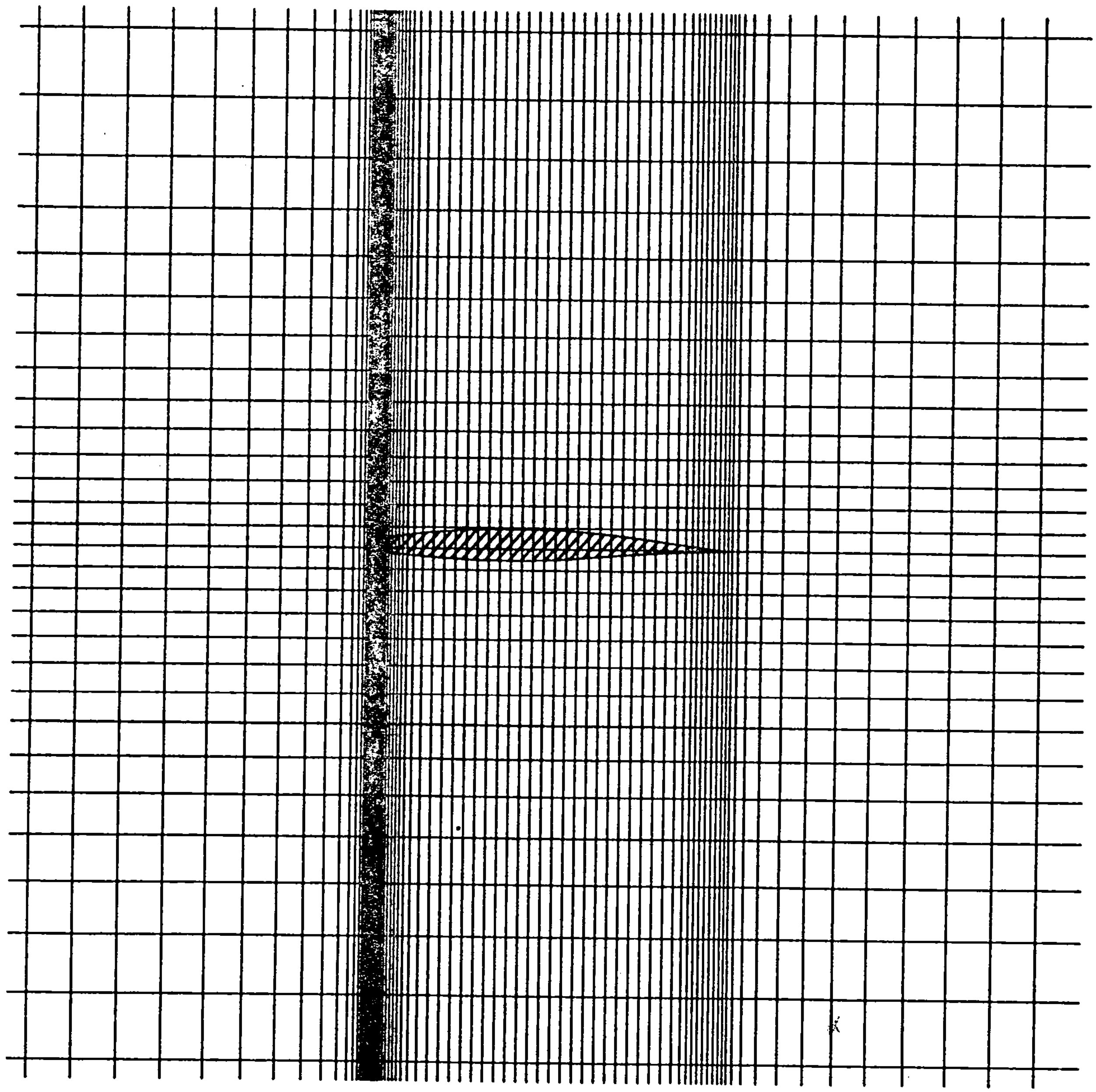

Fig. 3 LTRAN2-HI default grid near the airfoil for $\delta = 0.005$.

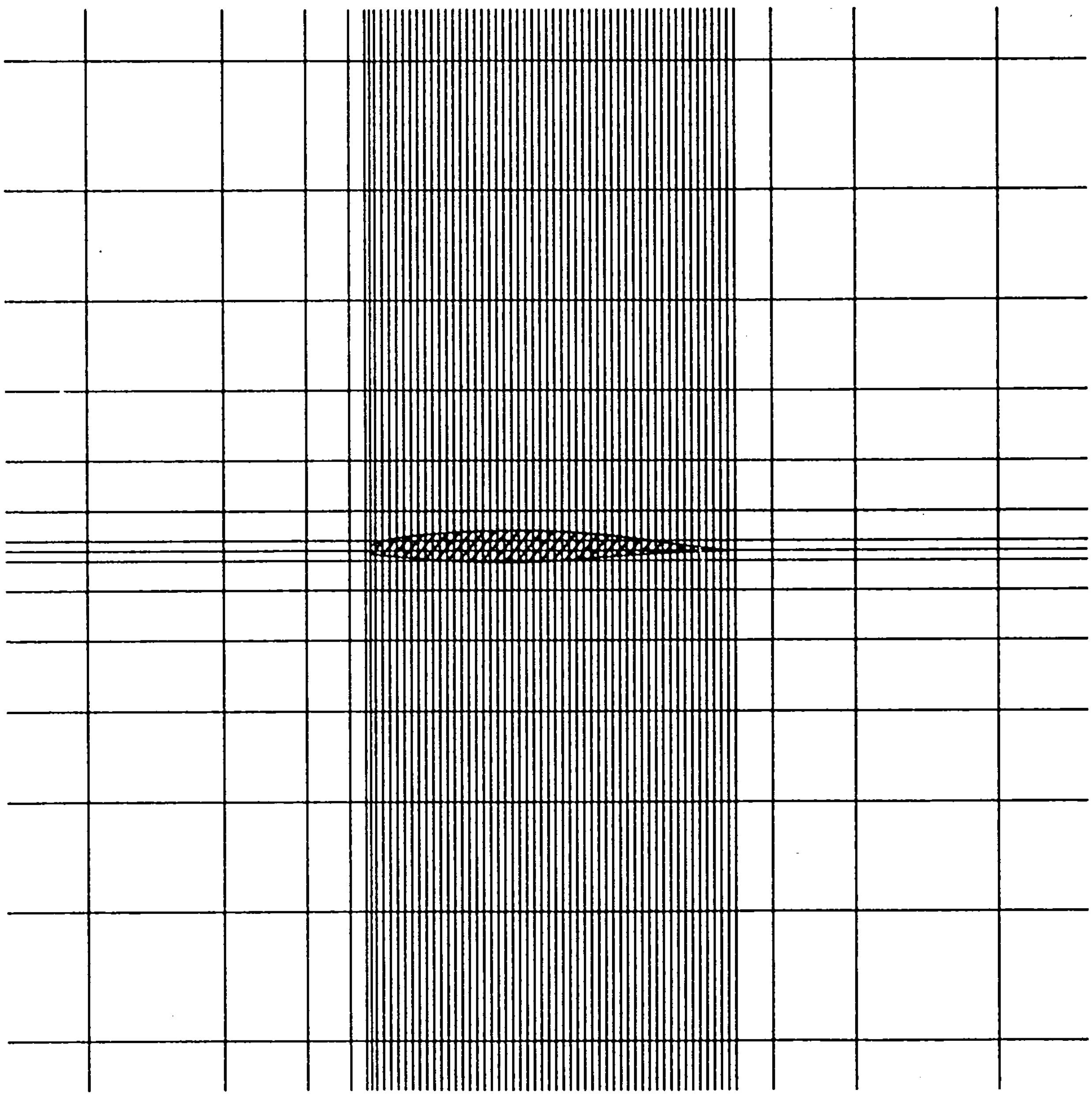

Fig. 4 XTRAN2L default grid near the airfoil.

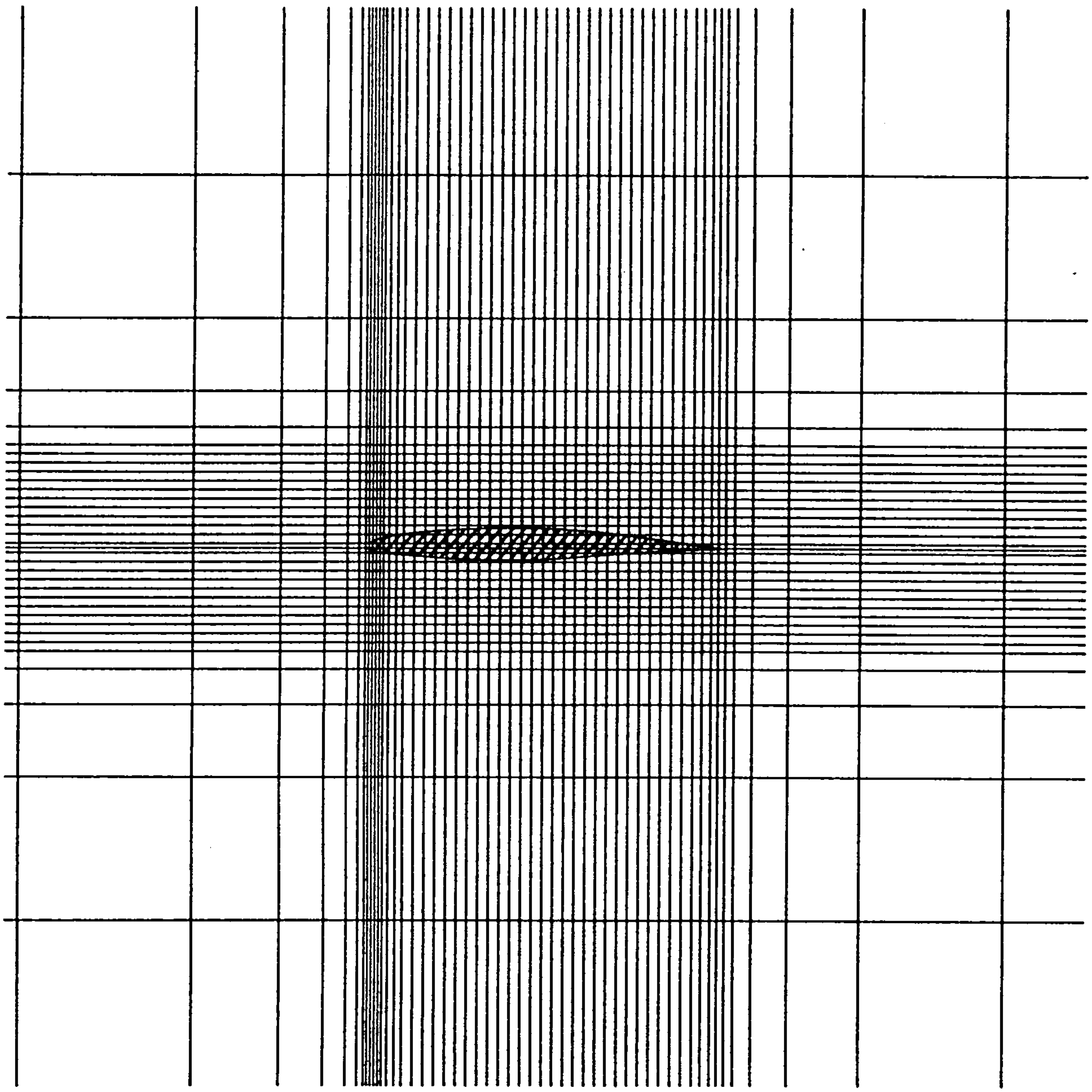

Fig. 5 XTRAN3S default root chord x,z grid near the airfoil.

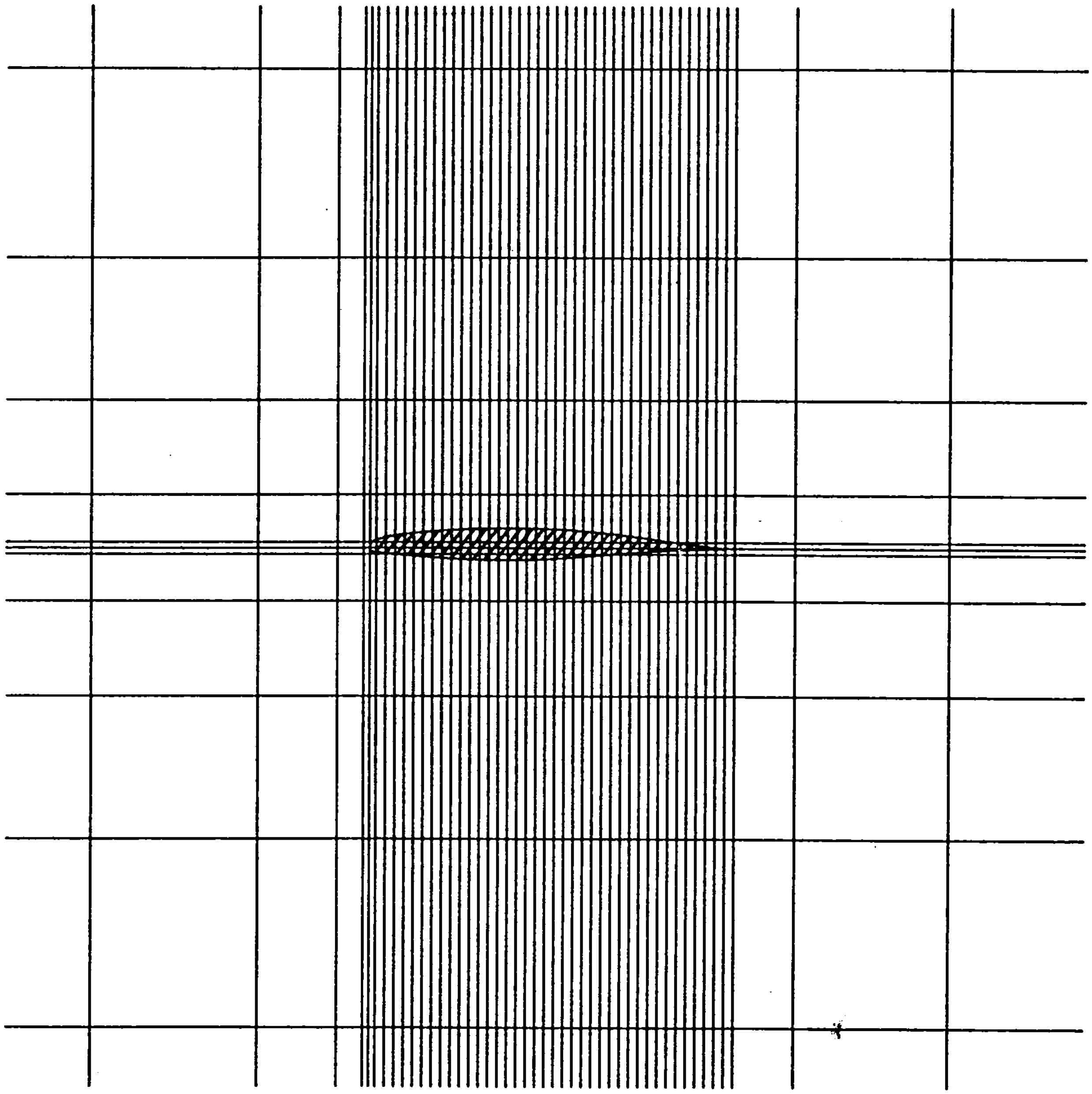

Fig. 6 Revised XTRAN3S root chord x,z grid near the airfoil.

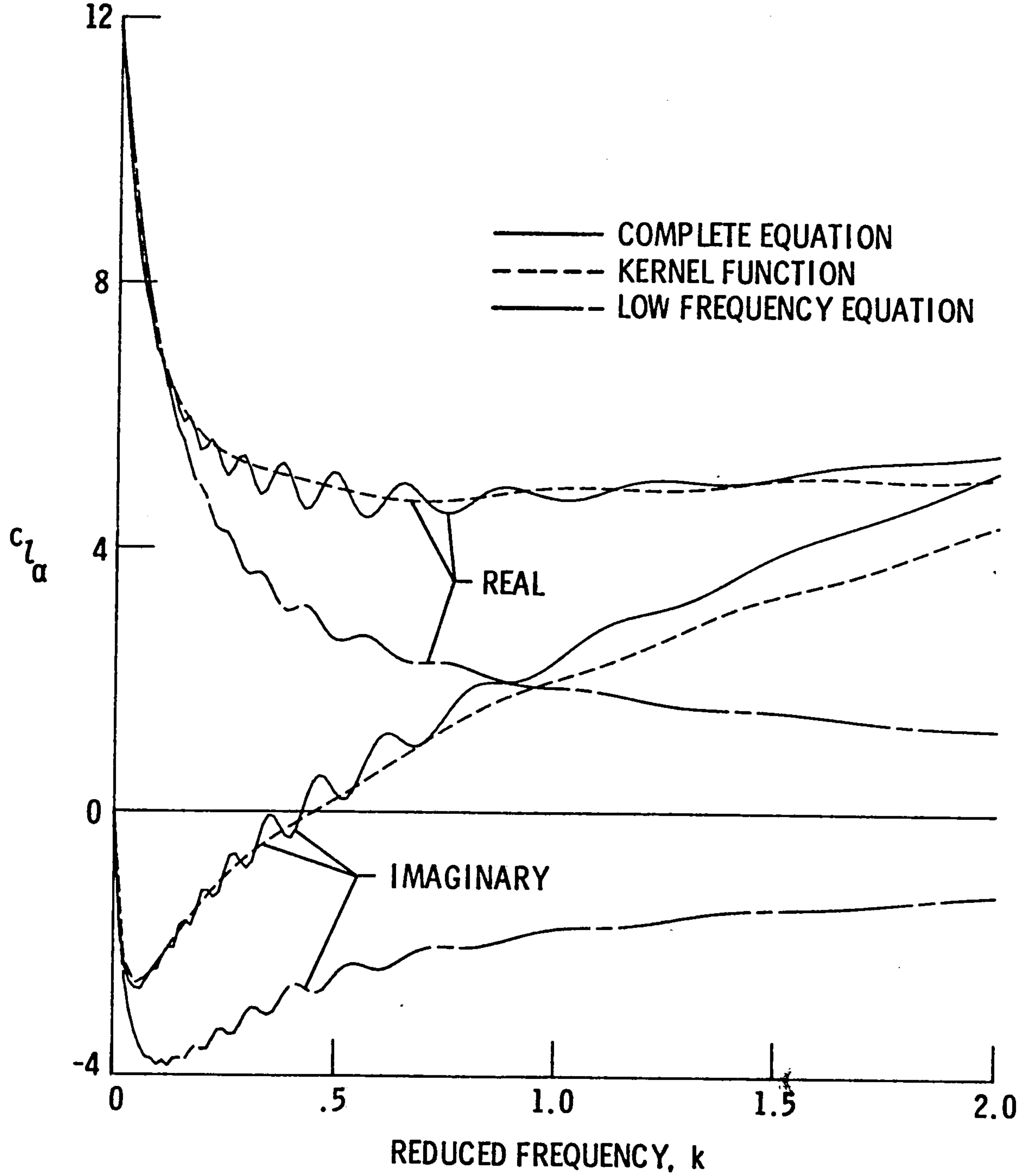

Fig. 7 Unsteady forces calculated for a flat plate airfoil using the LTRAN-NLR default grid, $M_\infty = 0.850$.

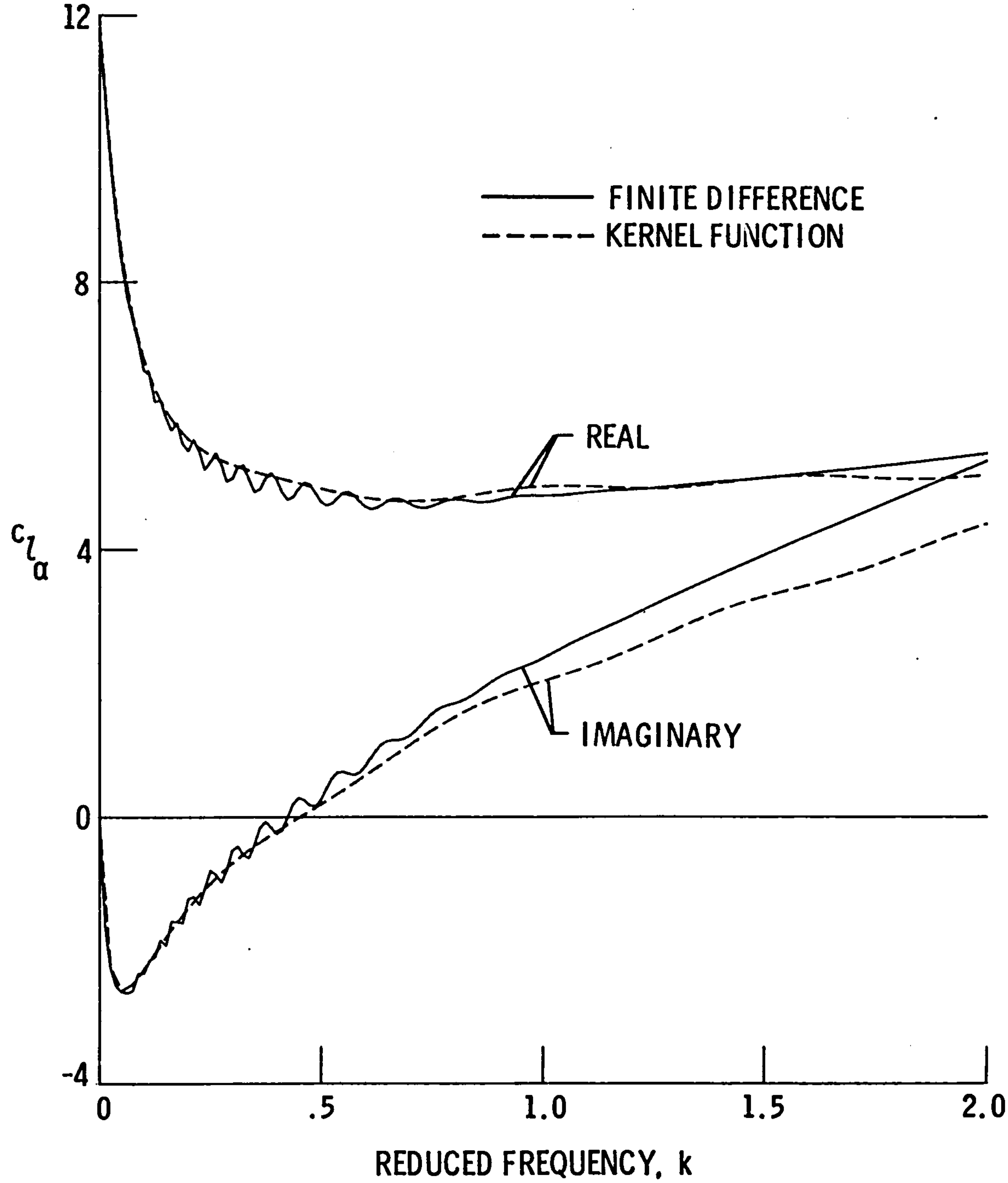

Fig. 8 Unsteady forces calculated for a flat plate airfoil using the LTRAN2-HI default grid, M_∞ = 0.850.

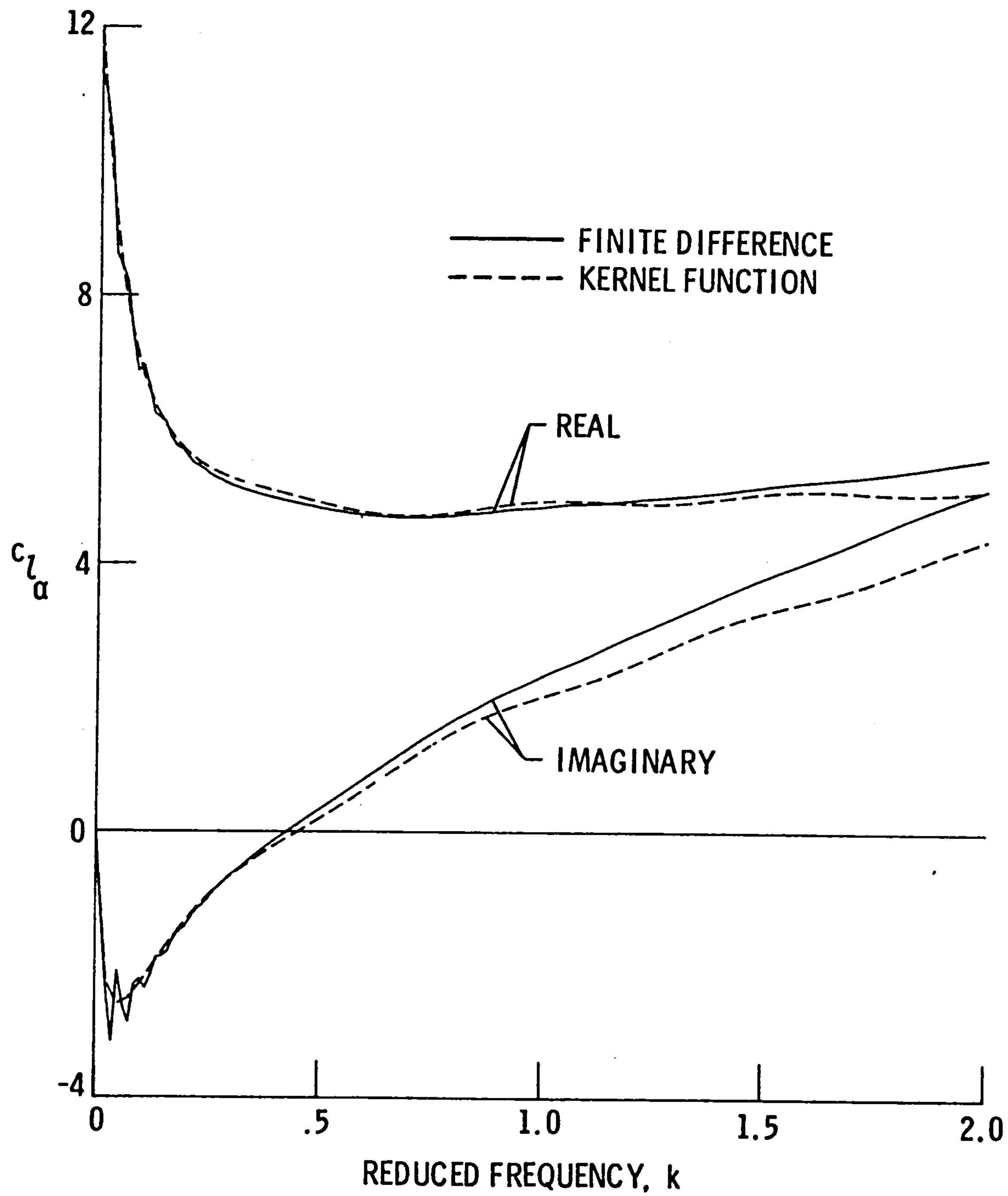

Fig. 9 Unsteady forces calculated for a flat plate airfoil using the XTRAN2L default grid with reflecting far-field boundary conditions, $M_\infty = 0.850$.

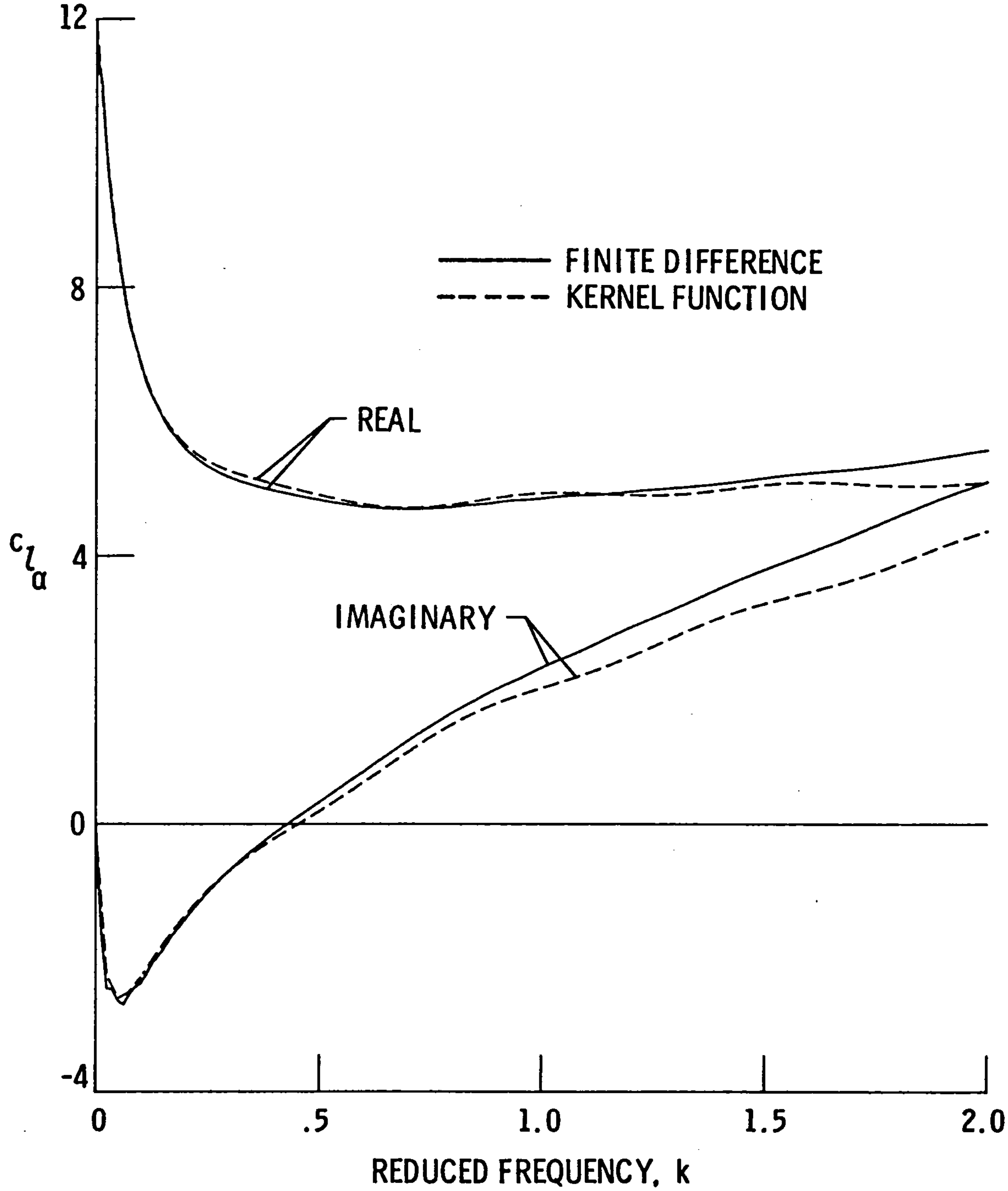

Fig. 10 Unsteady forces calculated for a flat plate airfoil using the XTRAN2L default grid with radiation far-field boundary conditions, $M_\infty = 0.850$.

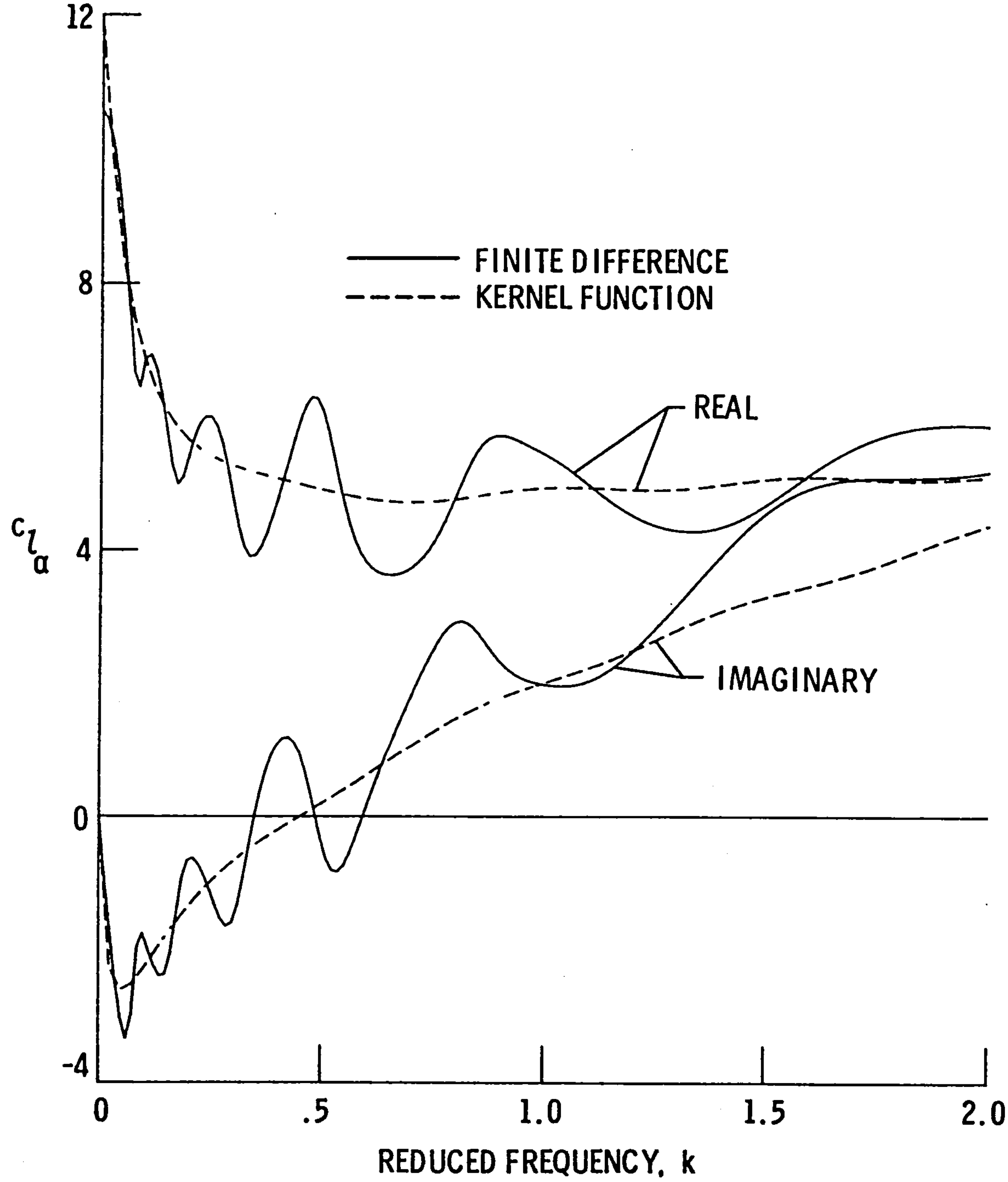

Fig. 11 Unsteady forces calculated for a flat plate airfoil using the default XTRAN3S root chord x,z grid, M_∞ = 0.850.

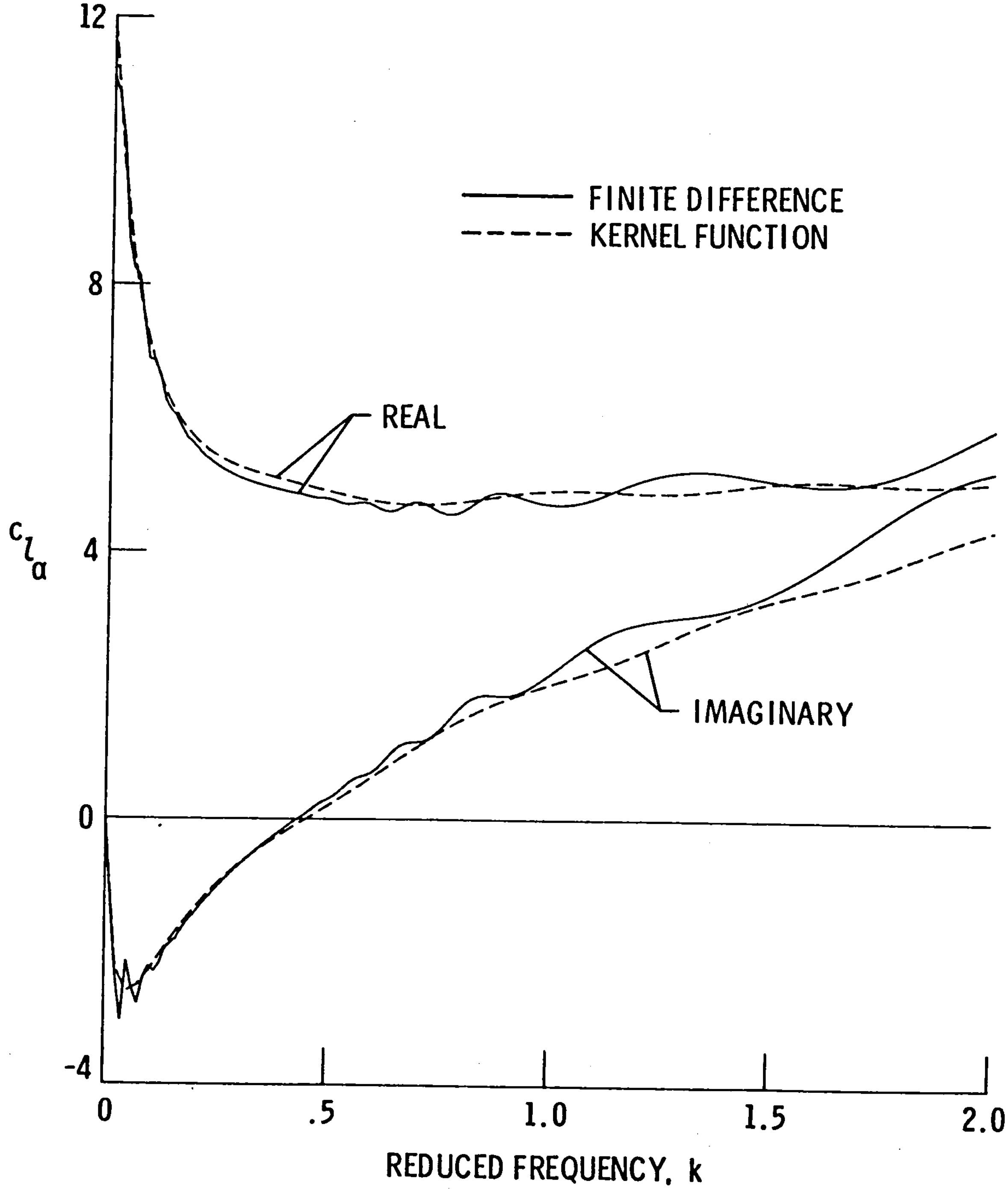

Fig. 12 Unsteady forces calculated for a flat plate airfoil using the revised XTRAN3S root chord x,z grid, $M_\infty = 0.850$.

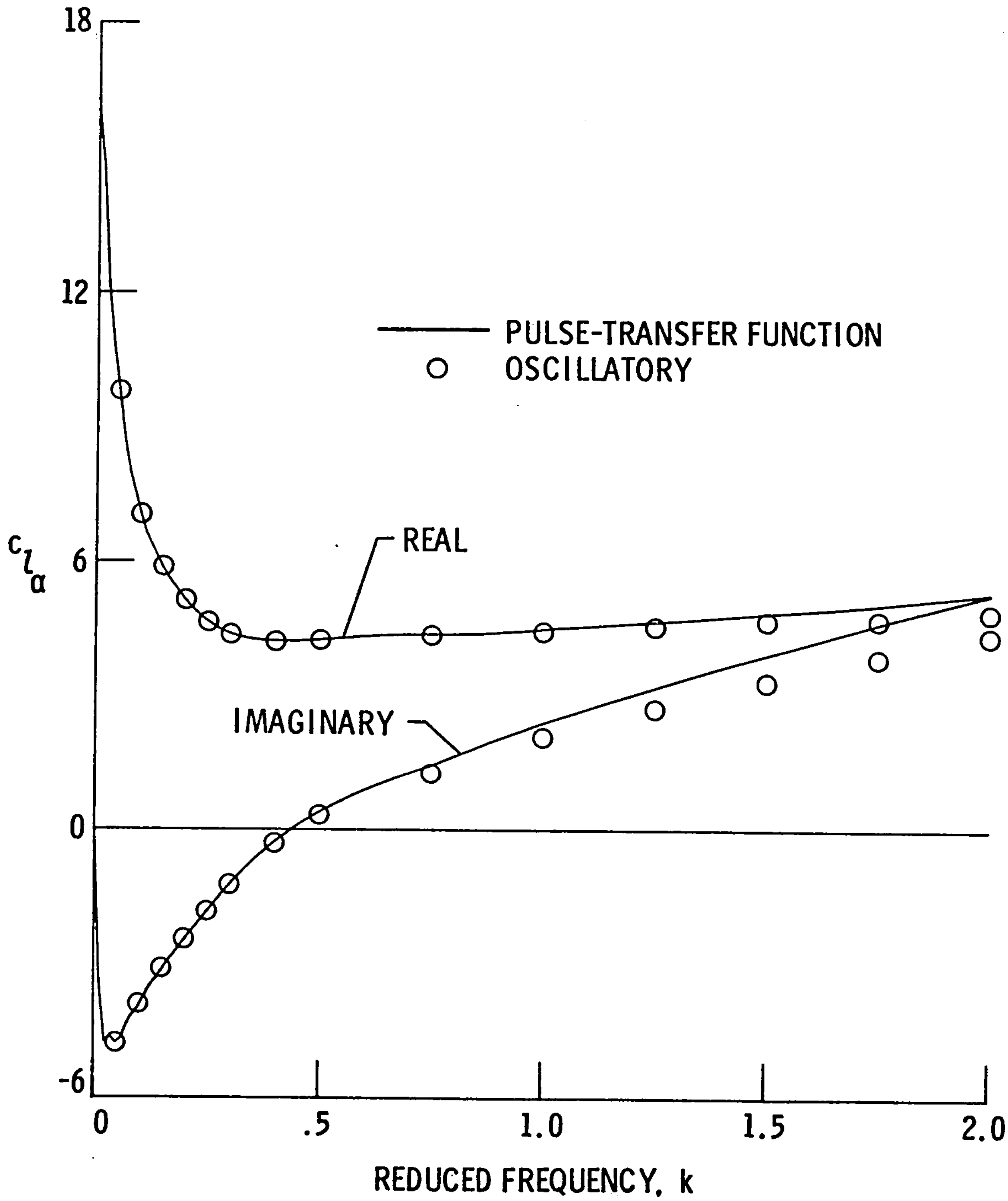

Fig. 13 Unsteady forces for a 6% parabolic arc airfoil calculated by pulse and oscillatory analyses; XTRAN2L default grid, $M_\infty = 0.850$.

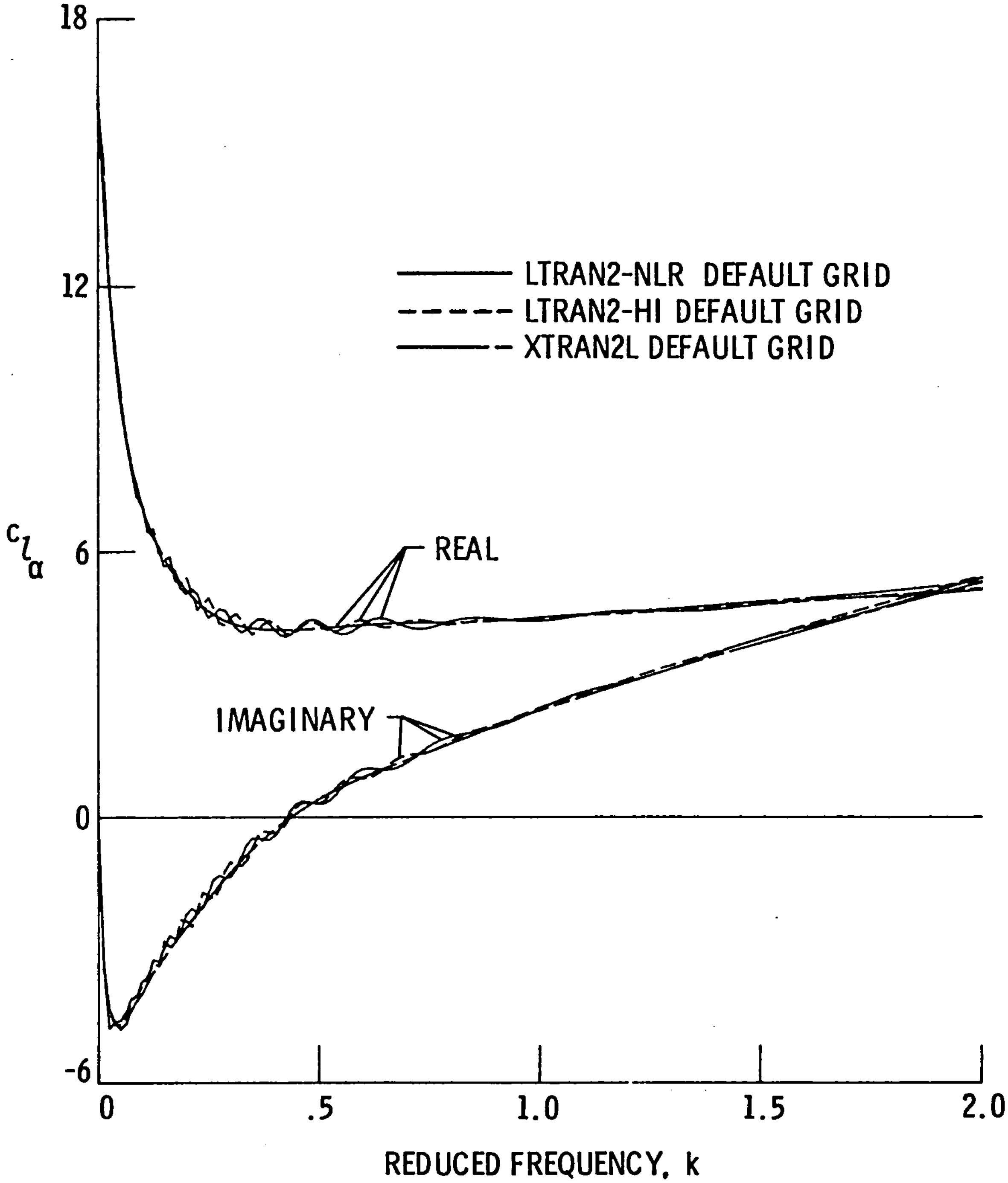

Fig. 14 c_{ℓ_α} for a 6% parabolic arc airfoil calculated using the LTRAN2-NLR, LTRAN2-HI and XTRAN2L default grids, M_∞ = 0.850.

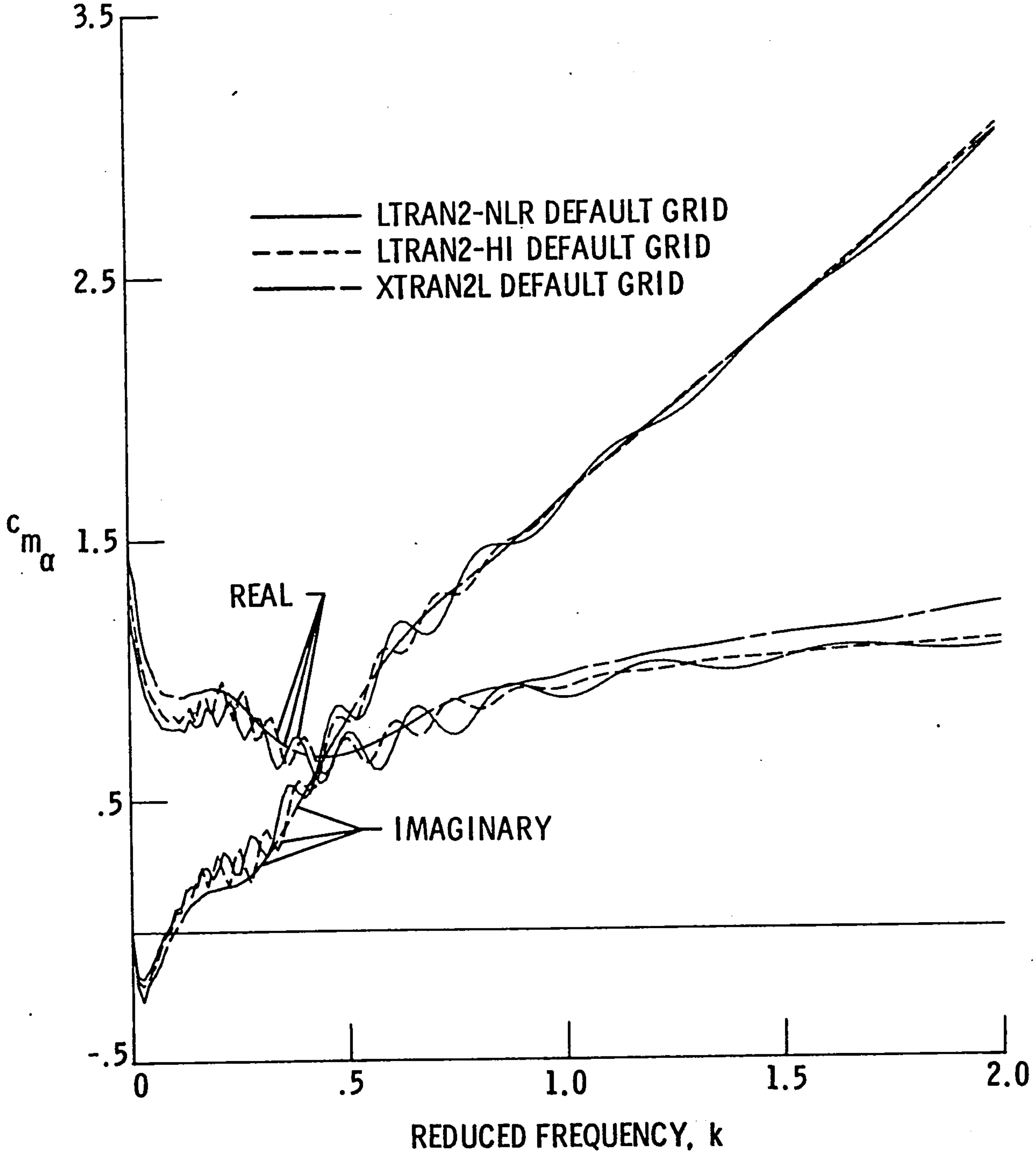

Fig. 15 c_{m_α} for a 6% parabolic arc airfoil calculated using the LTRAN2-NLR, LTRAN2-HI and XTRAN2L default grids, M_∞ = 0.850.

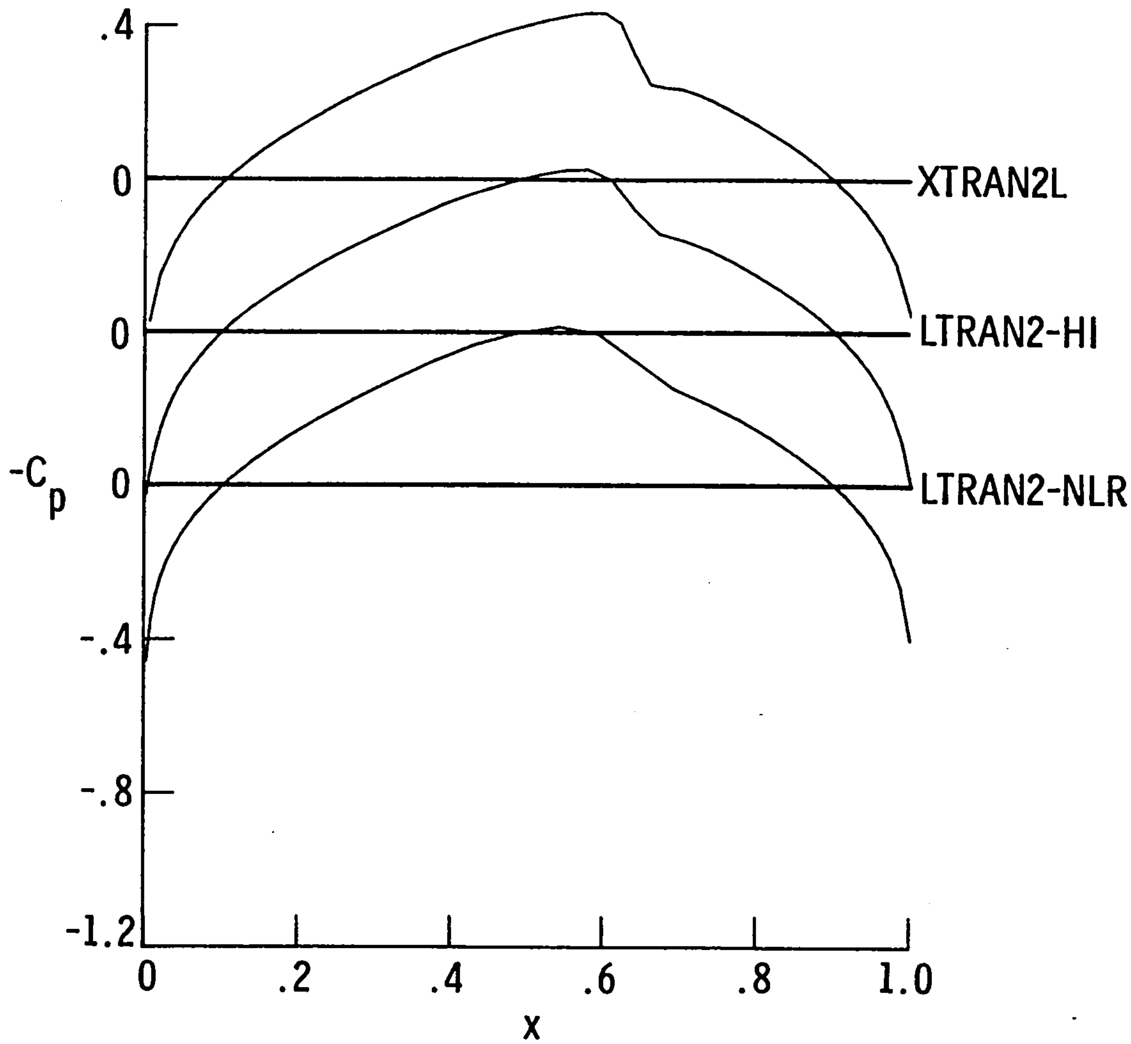

Fig. 16 Steady-state pressure distributions for a 6% parabolic arc airfoil calculated using the LTRAN2-NLR, LTRAN2-HI and XTRAN2L default grids, M_∞ = 0.850.

1. Report No.	2. Government Accession No.	3. Recipient's Catalog No.
NASA TM 84583		

4. Title and Subtitle
An Exploratory Study of Finite Difference Grids for Transonic Unsteady Aerodynamics

5. Report Date
December 1982

6. Performing Organization Code
505-33-43-09

7. Author(s)
David A. Seidel, Robert M. Bennett, and Woodrow Whitlow, Jr

8. Performing Organization Report No.

9. Performing Organization Name and Address
NASA Langley Research Center
Hampton, VA 23665

10. Work Unit No.

11. Contract or Grant No.

13. Type of Report and Period Covered
Technical Memorandum

12. Sponsoring Agency Name and Address
National Aeronautics and Space Administration
Washington, DC 20546

14. Sponsoring Agency Code

15. Supplementary Notes Unrestricted version of this paper will be presented at the 21st AIAA Aerospace Sciences Meeting, Reno, Nevada, January 10-13, 1983. AIAA Paper No. 83-0503

16. Abstract
Unsteady aerodynamic forces are calculated by the XTRAN2L finite difference program which solves the complete two-dimensional unsteady transonic small perturbation equation. The unsteady forces are obtained using a pulse-transfer function technique which assumes the flow field behaves in a locally-linear fashion about a mean condition. Forces are calculated for a linear flat plate using the default grids from the LTRAN2-NLR, LTRAN2-HI, and XTRAN3S programs. The forces are compared to the exact theoretical values for flat plate, and grid-generated boundary and internal numerical reflections are observed to cause significant errors in the unsteady airloads. Grids are presented that alleviate the reflections while reducing computational time up to fifty-three percent and program size up to twenty-eight percent. Forces are presented for a six percent thick parabolic arc airfoil which demonstrate that the transform technique may be successfully applied to non-linear transonic flows.

17. Key Words (Suggested by Author(s))
Finite Difference
Transonic Small Perturbation Equation
Grids
Unsteady Aerodynamics

18. Distribution Statement
[redacted]

Subject Category 02

19. Security Classif. (of this report)	20. Security Classif. (of this page)	21. No. of Pages	22. Price
Unclassified	Unclassified	38	

*Available: NASA's Industrial Applications Centers